6A.4 REFLECTIVE STORM TOPS: A SATELLITE METHOD FOR INFERRING THUNDERSTORM TOP MICROPHYSICAL STRUCTURE

Daniel T. Lindsey[1*] and Louie Grasso[2]
[1]NOAA/NESDIS/ORA/RAMMB
Fort Collins, Colorado
[2]Cooperative Institute for Research in the Atmosphere
Fort Collins, Colorado

1. INTRODUCTION

Satellite observations of thunderstorms have been widely documented since the launch of Geostationary Operational Environmental Satellites (GOES) in the 1970's. The current generation of GOES satellites have several added capabilities, including the addition of a channel centered near 3.9 µm, within the shortwave infrared portion of the electromagnetic spectrum. During the daytime, satellite-observed radiances at this channel include an emitted thermal component and a reflected solar component. For sufficiently optically thick clouds, the thermal component can be approximated by assuming the emitting temperature is the same at 3.9 µm as at 10.7 µm (GOES channel 4). Given observed 3.9 µm radiance, it is then possible to calculate the 3.9 µm solar reflected component. This is often represented as an albedo, or the percent of incoming solar radiation at 3.9 µm which is reflected back to the satellite.

Setvák and Doswell (1991) first noted, using advanced very high resolution radiometer (AVHRR) data, that some thunderstorm tops have enhanced solar reflectivity in the shortwave infrared portion of the spectrum. They suggest that differences in shortwave albedo may be due to differences in microphysical structure at cloud-top. It is well documented that liquid water clouds are more effective reflectors than ice clouds (e.g., Turk et al. 1998). However, thunderstorm tops often exist at temperatures well below -40 ˚C, meaning their composition is dominated by ice crystals. Differences in the size distributions of these ice crystals have an effect on shortwave infrared reflectivity: research has shown that more numerous smaller crystals tend to be more effective reflectors (Melani et al. 2003a,b). As a result, satellite detection of a "reflective" thunderstorm top implies that its anvil is composed of relatively small and numerous ice crystals, and this may provide information about internal thunderstorm structure (Setvák et al. 2003).

*Corresponding author address: Daniel T. Lindsey, CIRA/Colorado State University, 1375 Campus Delivery, Ft. Collins, CO 80523-1375; email: lindsey@cira.colostate.edu

Examples of thunderstorms with relatively high and low shortwave albedo are given in Figures 1a and 1b, respectively. Both of these days resulted in significant severe weather. Values of shortwave albedo for storms in Fig. 1a approach 15%, while values in Fig. 1b are generally less than 5%.

a)

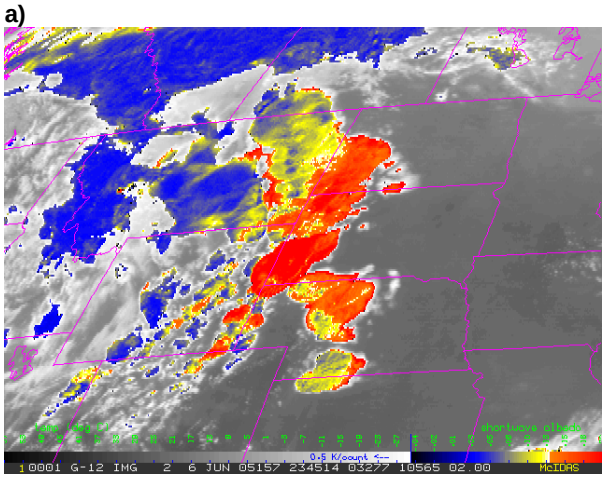

b)

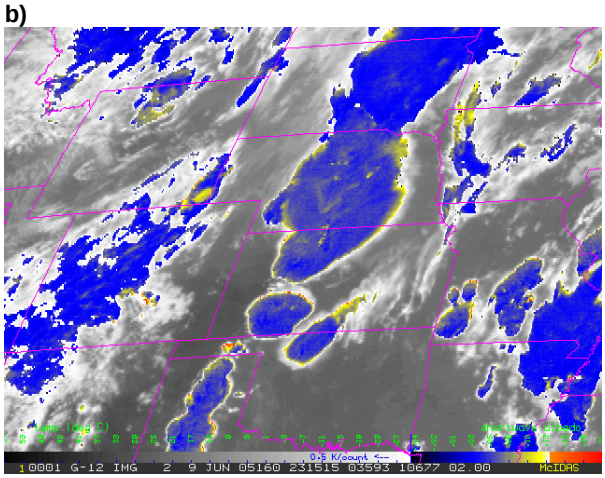

Figure 1. GOES-12 channel 4 (10.7 µm) for brightness temperatures greater than -30˚ C, and shortwave (3.9 µm) albedo for brightess temperatures less than -30˚ C (colors), for a) 6 June 2005 at 2345 UTC, and b) 9 June

2005 at 2315 UTC. Warmer colors indicate cold cloud tops with relatively large shortwave albedo values.

The primary goals of this study are to look at this reflective thunderstorm top phenomenon from a climatological perspective and seek mechanisms for the existence of small ice at cloud top. An explanation for significant differences in cloud-top shortwave albedo between two storms (as in Fig. 1) is sought. Section 2 will describe a climatological study of reflective ice clouds over the US; section 3 presents results of a statistical study using reanalysis data; section 4 describes modeling results linking ice crystal size to shortwave albedo; section 5 offers conclusions and areas for future work.

2. REFLECTIVE ICE CLOUD CLIMATOLOGY

GOES-10 and GOES-12 data were analyzed every 2 hours from September 2003 through August 2004. Channel 4 (10.7 μm) and channel 2 (3.9 μm) radiances were used to calculate the shortwave albedo at every pixel within the domain for the entire year. Only times when the solar zenith angle was less than 68 degrees were included, since the albedo calculation has large errors near sunrise and sunset, and is impossible at night. The analysis was also limited to cloudy pixels with 10.7 μm brightness temperatures colder than -40˚ C. This was an attempt to eliminate thin cirrus, and ensured that the clouds were composed almost entirely of ice crystals (no liquid water droplets).

Figure 2a shows the results of the climatological study from GOES-12. Contours represent the percent of ice cloud pixels (defined above) whose 3.9 μm albedo is greater than 5%. Shortwave albedo was calculated following the method outlined by Setvák and Doswell (1991). The choice of the 5% threshold was arbitrary; changing the threshold had a very small effect on the resulting geographical distribution. Pixels were grouped into 1x1 degree (lat/lon) boxes before the percentages were computed. The maximum over the high plains and moutainous regions is obvious. Areas east of ~100˚ W longitude have values between zero and 5%, meaning highly reflective clouds are significantly less common there. Figure 2b is similar to Fig. 2a, except for the GOES-10 domain. Values throughout the west are larger, and maxima are evident in eastern Colorado, northwest Montana, and southeastern California. These areas are all downwind of major mountain ranges, suggesting that high terrain may play an important role in the mechanism for generating small ice at cloud top. Values over eastern Colorado are slightly smaller from the GOES-10 perspective compared to those from GOES-12 (Fig. 2a). This may be due to preferential forward scattering when the sun is approaching the western horizon and the convective activity reaches a maximum in late afternoon.

a)

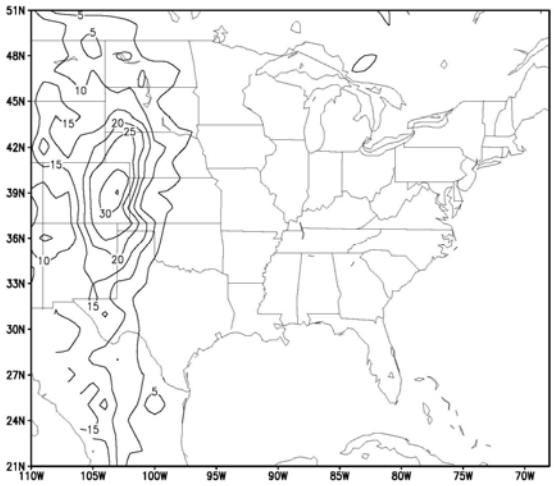

b)

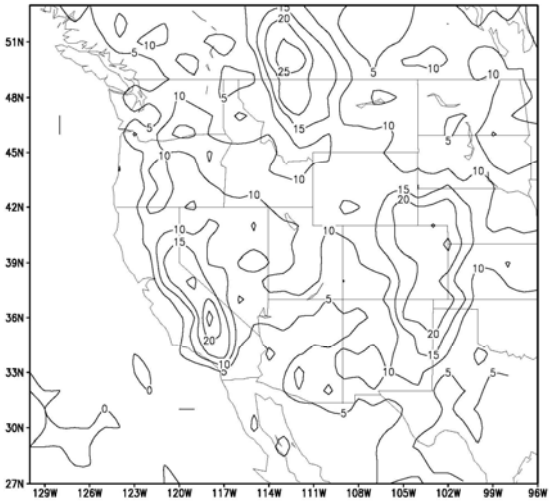

Figure 2. Percent of ice clouds whose 3.9 μm albedo exceeds 5% from GOES-12 (a) and GOES-10 (b), from Sep. 2003 - Aug. 2004, for times when the solar zenith angle exceeds 68˚.

Figures 3a,b show results from the same climatological study, but from a slightly different perspective. Annual mean values of shortwave albedo for ice clouds are contoured. The same geographical maxima observed in Fig. 2 are visible here, and the mean values are roughly 2.5% in most of the eastern US compared to over 5% in eastern Colorado. This difference may appear slight, but as will be shown later, a small difference in shortwave albedo implies a fairly large difference in cloud-top ice crystal size.

a)

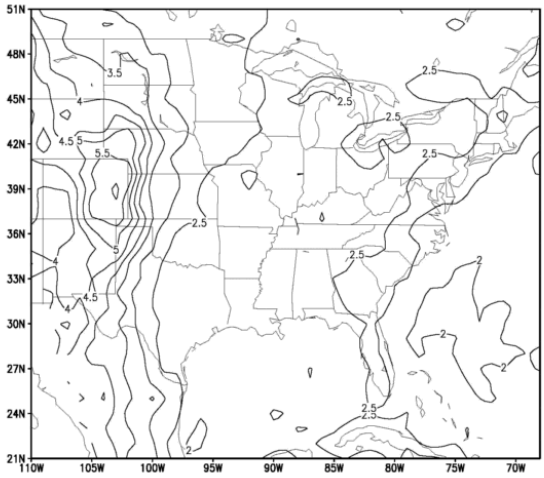

b)

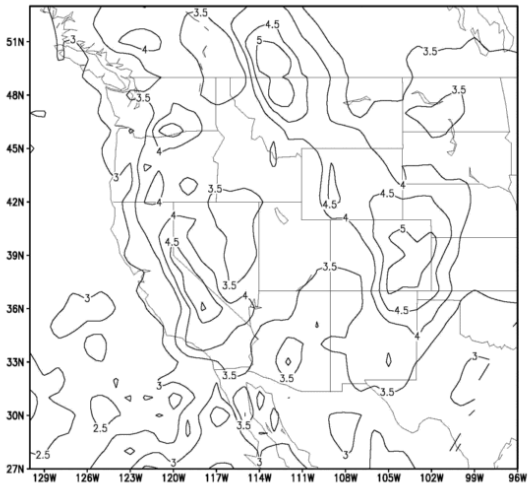

Figure 3. Mean shortwave albedo of ice clouds from GOES-12 (a) and GOES-10 (b), from Sep. 2003 - Aug. 2004, for times when the solar zenith angle exceeds 68˚.

Analysis of the monthly trend of reflective tops for the longitudinal band between 105W - 95W (Fig. 4a,b) reveals a maximum during the summer months and a secondary maximum during the winter, with minima in the fall and spring. The summertime maximum is primarily associated with convection, while the secondary winter maximum is likely associated with mountain wave clouds, which also tend to be relatively reflective. Ice clouds with shortwave albedos greater than 5% east of 95W are quite rare, especially during the summer (Fig. 4a). The western part of the continental US has more reflective ice clouds on average (see also Fig. 3b). The band between 105W - 95W shows the same trend with GOES-10 as GOES-12, while the band further west have more complex month-to-month variability. Current thinking is that the western maxima are dominated by mountain wave clouds, since the maxima lie at or just downstream of major mountain ranges (Fig. 3b).

a)

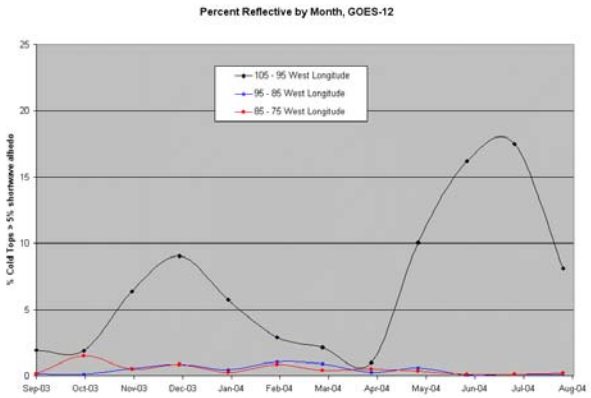

b)

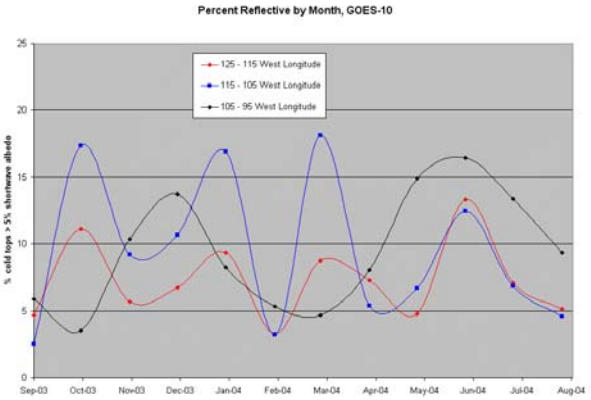

Figure 4. Monthly distribution of percent of cold pixels exceeding 5% shortwave albedo, divided into longitudinal bands, for a) GOES-12 and b) GOES-10.

3. STATISTICAL ANALYSIS

In an effort to understand the physical basis behind the strong geographical signal in Fig. 2a, a statistical method was applied to several theromdynamic parameters in the following way. First, a domain was chosen from Fig. 1a roughly within the 15% contour, or between approximately 30˚-45˚ N. latitude and between 100˚-110˚ W. longitude. Satellite data during the summer months (June, July, August) of 2003 and 2004 was analyzed, and 16 convective days having a large percentage of reflective thunderstorm tops (hereafter referred to as "reflective days") and 16 convective days having a low percentage of reflective thunderstorm tops ("non-reflective days") were selected. Though not used in this particular analysis, days similar to those in Figures 1a and 1b are typical examples of a reflective day and a non-reflective day, respectively.

For each of the 16 reflective and 16 non-reflective days, grid points from the North American Regional Reanalysis (NARR) dataset falling within an area containing the convective clouds were selected. NARR data is similar to the NCEP/NCAR reanalysis, but includes data from more sources. Additionally, grid spacing is 32-km, so between 500 and 1000 grid points were available for each day, depending on the size of box chosen. Grid point values at 0000 UTC of temperature, dewpoint, and wind from the surface to 100 mb were averaged for each of the 16 days. These mean profiles were then averaged for the reflective days and non-reflective days, producing two final mean profiles. These are given in Figure 5.

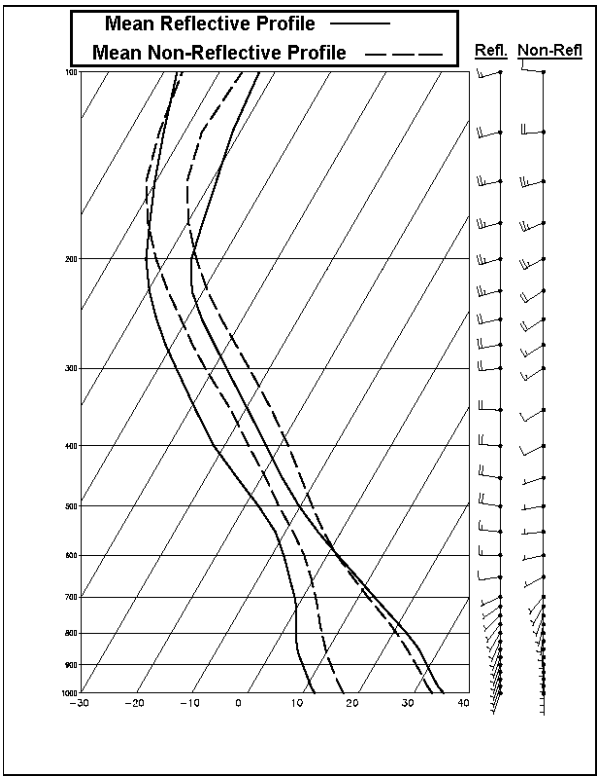

Figure 5. Mean temperature (right) and dewpoint (left) profiles for the reflective (solid) and non-reflective (dashed) cases, along with mean wind profiles, plotted on a traditional skew-T/log-p diagram. A full wind barb represents 10 knots.

There are several important differences between these two mean profiles. First, the relative humidity throughout the reflective profile is lower, especially in the lowest 400 mb. A larger temperature/dewpoint spread near the surface suggests a fairly dry boundary layer is supportive of reflective thunderstorm tops. (This can also be inferred by looking at the climatology maps in Figure 2). Secondly, and possibly more importantly, the 800-300 mb lapse rate is noticeably steeper in the reflective case. This environment would promote more instability and stronger updrafts. Finally, the mid-level westerlies are stronger in the reflective case.

To get a more quantitative understanding of the results, values of several variables were collected at each grid point, and means and standard deviations were calculated for each of the 32 days. Next, the resulting means were averaged together for each case (reflective and non-reflective), and the standard deviations were also averaged. Results are given in Table 1. To estimate significance, a difference of means t-test was performed, using the mean standard deviations calculated above. Variables in Table 1 with greater than 95% significance are shaded in light gray; those exceeding 99% significance are shaded in dark gray. It should be noted that standard deviations were also calculated for the daily distributions of means (as opposed to the grid point mean for each day), and these were lower than the average standard deviations, so the larger, more conservative estimates were used.

	Reflective Case Mean	Non-Reflective Case Mean
CAPE (J/kg)	567	219
Precipitable Water (mm)	17.7	23.1
Surface Temperature (°C)	28.2	26.1
Surface Dew Point (°C)	4.5	7.2
700mb RH (%)	42	56
500mb RH (%)	58	65
800-500mb Lapse Rate (°C per km)	8.5	7.4
Sfc - 500mb Zonal Shear (ms^{-1})	9.9	2.3

Table1. Means for several variables for the 16 reflective days and 16 non-reflective days. Light gray shading indicates the difference of means exceeds 95% significance; dark gray for difference of means exceeding 99% significance.

The CAPE for the reflective case is over twice the value than for the non-reflective case, verifying that instability is greater in the reflective situation (even though convection was observed in both cases). Precipitable water values are smaller and 700mb relative humidity values are lower for the reflective case, further underscoring the possible importance of relatively dry air. Lapse rates are significantly steeper in the reflective case (the standard deviations for lapse rate were very small), and the surface-to-500-mb zonal shear is much larger on reflective days.

4. RELATIONSHIP BETWEEN ICE CRYSTAL SIZE AND SHORTWAVE ALBEDO

In order to investigate the relationship between cloud-top ice crystal size and 3.9 μm albedo an observational operator (Grasso and Greenwald 2004) was used to simulate GOES brightness temperatures for a homogeneous ice cloud. The observational operator is partitioned into three sections. The first section computes gaseous transmission at a specified wavelength. Next, optical properties -- single scatter albedo, extinction, and asymmetry -- of the cloud are calculated. Finally, bulk optical properties are sent to

radiative transfer routines for brightness temperature computations.

The top of the ice cloud composed of pristine ice was placed at 12-km AGL, near the tropopause, and the thickness was set to 2-km. Mass mixing ratio and number concentration were then varied to produce a range of ice crystal mean diameters for an assumed Gamma size distribution; for each mean diameter, the 3.9 µm albedo was calculated, and the results are plotted in Figure 6.

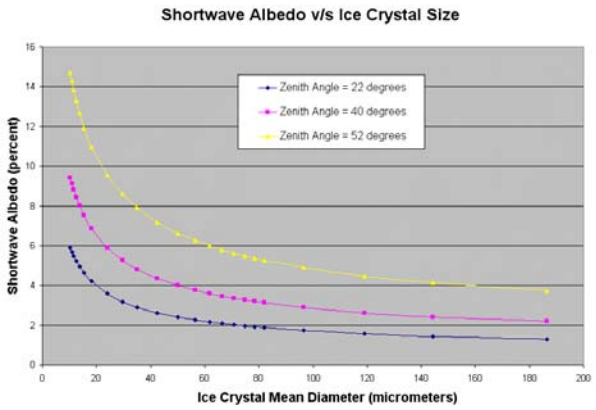

Figure 6. Model results for 2-km-thick cloud composed of pristine ice, for 3 solar zenith angles.

For a given solar zenith angle, the shortwave albedo is fairly insensitive to ice crystal size for diameters greater than about 80 µm, but for smaller values, the shortwave albedo increases dramatically. According to the model, increasing the solar zenith angle (as the sun approaches the horizon) also produces a dramatic increase in shortwave albedo for a give ice crystal size. The important result is that ice crystal cloud reflectivity increases dramatically for small ice crystal sizes. It should also be noted that the model predicted 10.7 µm brightness temperatures near 220 K (approximately the tropopause temperature) for all ice crystal sizes. This means that the cloud was sufficiently optically thick to prevent any emitted terrestrial radiation from penetrating it.

5. CONCLUSIONS AND FUTURE WORK

Preliminary results of this study are quite encouraging. The geographical distribution of highly reflective ice clouds has never been documented. Statistical results presented here suggest that over the high plains, relatively dry, unstable environments favor thunderstorms with reflective cloud tops. A physical mechanism linking these conditions with smaller ice crystal sizes at cloud top is not known. Possibilities include cloud condensation nuclei and ice nuclei distributions, dry air entrainment into the updraft, homogeneous nucleation of tiny cloud droplets within a strong updraft, and possibly others. The authors welcome additional ideas (see email address on page 1).

Work is currently underway to improve the model simulations presented in Section 4. We plan to use more sophisticated ways of representing the scattering phase function, along with allowing the ice crystal habit to vary. The eventual goal is to obtain an accurate relationship between shortwave albedo and ice crystal size/habit, so that satellite measurements of shortwave albedo may provide information about cloud-top microphysical structure. This may then be used to infer internal thunderstorm processes (like updraft strength, etc.).

Finally, a link between reflective storm tops and instability (Table 1) suggests that the GOES shortwave infrared channel may be used to locate storms more likely to produce severe weather. A combination of GOES data with other environmental variables, like CAPE and shear, may yield a useful thunderstorm nowcasting tool. But first, a statistical link between reflective storms and severe weather will need to be established.

6. REFERENCES

Grasso, L. D., and T. J. Greenwald, 2004: Analysis of 10.7-µm brightness temperatures of a simulated thunderstorm with two-moment microphysics. *Mon. Wea. Rev.*, **132**, 815-825.

Melani, S., E. Cattani, V. Levizzani, M. Cervino, and F. Torricella, 2003: Radiative effects of simulated cirrus clouds on top of a deep convective storm in METEOSAT second generation SEVIRI channels. *Meteorol. Atmos. Phys.*, **83**, 109-122.

———, E. Cattani, F. Torricella, and V. Levizzani, 2003: Characterization of plumes on top of a deep convective storm using AVHRR imagery and radiative transfer model simulations. *Atmos. Res.*, **67-68**, 485-499.

Setvák, M., and C. A. Doswell III, 1991: The AVHRR channel 3 cloud top reflectivity of convective storms. *Mon. Wea. Rev.*, **119**, 841-847.

————, R. M. Rabin, C. A. Doswell III, V. Levizzani, 2003: Satellite observations of convective storm tops in the 1.6, 3.7, and 3.9 µm spectral bands. *Atmos. Res.*, **66-67,** 607-627.

Turk, J., J. Vivekanandan, T. Lee, P. Durkee, and K. Nielsen, 1998: Derivation and applications of near-infrared cloud reflectances from GOES-8 and GOES-9. *J. Appl. Meteor.*, **37**, 819-831.